Chen et al., J Material Sci Eng 2018, 7:3
DOI: 10.4172/2169-0022.1000453

Journal of Material Sciences & Engineering

Research Article Open Access

Characterization of Correlated Calcium Dynamics in Astrocytes in PCL Scaffold: Application of Wavelet Transform Coherence

Bo Chen[1], Fenghua Tian[1], Nicole Hashemi[2], Marilyn McNamara[2] and Michael Cho[1]*

[1]*Department of Bioengineering, University of Texas at Arlington, Arlington, TX, USA*
[2]*Department of Mechanical Engineering, Iowa State University, Ames, IA, USA*

Abstract

While 2D culture models have been used extensively to elucidate the cell-to-cell communication, they do not recapitulate fully the 3D characteristics of microenvironment in vivo, e.g., polarized cell attachment and generally confer a considerably stiffer substrate than the endogenous extracellular matrix. Development of fibrous scaffolds that can better mimic the native microenvironment and improve the spatial arrangement of seeded cells should foster experimental strategies to monitor and determine the 3D cell-to-cell communication. In this study, poly(ε-caprolactone) (PCL) fibers were fabricated in different sizes using a microfluidic platform and spatially arranged to create a suitable 3D microenvironment in order to investigate the cell viability and calcium signaling in mouse astrocytes. A powerful algorithm, referred to as wavelet transform coherence (WTC), was applied to establish the correlation between astrocytes that were seeded on the PCL fiber. As expected, two astrocytes that appeared to be in physical contact showed high correlation, whereas two astrocytes seeded within a few cell lengths but not in physical contact showed negligible correlation. The WTC correlation analysis of a cluster of six astrocytes seeded on a single PCL fiber led to surprising results that the cells can communicate over many cell lengths without being in physical contact. More systematic studies using spatially controlled 3D microenvironment will likely help unravel the intricate cell communication mechanisms.

Keywords: Correlated calcium dynamics; Astrocytes; PCL fibers; Wavelet transform coherence

Introduction

Calcium ion (Ca^{2+}) is a highly versatile biological intracellular signaling mediator for many cellular processes including proliferation, viability, and differentiation [1]. Ca^{2+} also has a direct role in controlling the expression patterns of its signaling systems that are constantly being remodeled in both normal and diseased tissues [2]. A recent study suggests that dysregulation of Ca^{2+} leads to neurodegeneration, which is prominent in blast-induced traumatic brain injury [3]. Intercellular calcium waves do propagate between neighboring cells, occur widely among different cell types [4-6], and therefore have generated attentions for many years. However, we are still at an early stage of understanding the function of such Ca^{2+} waves and need to better grasp the complexity of calcium signaling [7]. Another layer of the complexity is attributed to a large number of studies that were performed using 2D cell culture systems that may not recapitulate the 3D spatial arrangement of cells in vivo. The 2D models do not capture, for example, the polarized cell attachment and generally confer a considerably stiffer substrate environment than the endogenous extracellular matrix (ECM).

Biocompatible polymers can be used to mimic the 3D ECM. Because of the good solubility, exceptional blend-compatibility and slower degradation rate, many polymers such as polyglycolide (PGA) and poly-D,L-lactide (PDLA) have been utilized to provide more relevant 3D ECM features. In addition, polycaprolactone (PCL) has stimulated extensive research of its potential application into cell migration [8,9], collagen fibrils mimicking [10], stem cell differentiation [11,12], neural stem cell navigation [13] and nerve tissue engineering [14-17]. Several fabrication techniques therefore have been developed to control PCL fibrous scaffolds. For example, the electrospinning technique is relatively easy to use and compatible with PCL. However, this method requires high voltages (5-50kv) to pull the charged solution, which might alter the properties of sensitive biological materials [18]. Microfluidics has emerged as an alternate methodology due to the compatibility with cells, proteins, and peptides as well as cost-effectiveness and simplicity [19,20]. For instance, microfluidic spinning is capable of creating highly controllable, continuously fabricated, cell-embedded or cell-seeded fibers [13,18,21]. This efficient, rapid, and low-cost technique does not require large sample sizes or extreme polymerization requirements [21]. Instead, it relies upon the use of microchannels as well as pre-gel and sheath solutions to help shape and solidify the resulting fiber [18,21,22]. Within the microfluidic regime, fluids flow in a laminar flow and exhibit low Reynolds' numbers, thereby allowing for diffusion to take place at the interface between the core and sheath fluids [21]. The microfluidic device utilized for the current study features four chevrons on the top and bottom of the main channel and has been documented at length elsewhere [18,21,22].

Astrocytes are abundantly found in the central nervous system (CNS), and they are critical in maintenance of neuronal cells as well as assistance in intracellular communication of neural pathways. We recently and systematically studied the cell viability, calcium dynamics, and oxidative stress of astrocytes exposed to mechanical trauma (e.g., microcavitation) [23,24]. One interesting question remained unanswered whether partially damaged astrocytes can be rescued by neighboring healthy cells. In this study, PCL fibers are fabricated in different sizes using a microfluidic platform and spatially arranged to create a 3D microenvironment in order to investigate the cell viability and calcium signaling in astrocytes. The propagation direction of calcium signaling is successfully guided along the PCL fibrous network,

***Corresponding author:** Michael Cho, Department of Bioengineering, University of Texas at Arlington, Arlington, TX, USA, Tel: 817-272-2965; E-mail: michael.cho@uta.edu

Received May 11, 2018; **Accepted** May 18, 2018; **Published** May 28, 2018

Citation: Chen B, Tian F, Hashemi N, McNamara M, Cho M (2018) Characterization of Correlated Calcium Dynamics in Astrocytes in PCL Scaffold: Application of Wavelet Transform Coherence. J Material Sci Eng 7: 453. doi: 10.4172/2169-0022.1000453

and a sophisticated mathematic model was applied to determine the cell-cell interaction through monitoring the calcium dynamics of astrocytes in 3D fibrous scaffold.

Materials and Method

Materials and cell cultures

Poly(ε-caprolactone) (PCL) (MW=80,000), polyethylene glycol (PEG) (MW=20,000), ethanol, Dulbecco's phosphate-buffered saline (DPBS), Hanks' balanced salt solution (HBSS), high glucose (4500 mg/L) Dulbecco modified Eagle's medium (DMEM), fetal bovine serum (FBS) and penicillin/streptomycin were all purchased from Sigma-Aldrich (St. Louis, MO). 2, 2, 2-Trifluoroethanol (TFE), used as the solvent for PCL, was obtained from Oakwood Chemical (West Columbia, SC). Entactin-Collagen IV-Laminin (ECL) was purchased from Millipore Corporation (Billerica, MA). NucBlue™ Live Ready Probes was obtained from Thermo Fisher Scientific (Waltham, MA). Mouse astrocytes C8-D1A were purchased from American Type Culture Collection (ATCC, Manassas, VA) and cultured with DMEM, 5% FBS, and 1% penicillin/streptomycin in a 37°C and 5% CO_2 incubator. When cells grew confluent between 70 to 90%, they were sub-cultured at the density of 50,000 cell seeded on 22 × 22 mm glass coverslips containing PCL fiber substrate (see below). Cells in 3D PCL scaffold were further cultured for additional several days prior to experimentation. Astrocytes from the passages 2 to 8 were used for the experiments.

Microfluidic fiber fabrication

Microfluidic devices were generated by the use of a SU8 photoresist-patterned silicon wafer, which was used to pattern polydimethylsiloxane (PDMS). The pattern of the microfluidic device has been previously described [21,22]. To create PCL fibers, a 5% PCL (w/v) solution in TFE and 5% PEG (w/v) was dissolved in deionized (DI) water and ethanol (1:1 ratio). The mixture was pumped into the microfluidic device using a double syringe pump (Cole-Parmer, Vernon Hills, IL). The fibers were released into a bath of the DI water and ethanol, where it was collected around a paper frame in the desired pattern.

PCL fiber substrate preparation

Pre-cleaned glass coverslips were rinsed in DI water, air-dried and treated with ultraviolet light sterilization. The microfibers were then attached to the coverslips using medical adhesive. Small droplets of medical adhesive were placed at opposite sides of the coverglass and a parallel array of microfibers placed across the coverglass and attached to the medical adhesive droplets. The microfibers were fixed at opposite ends and loose across the middle of the coverglass. The coverglass and PCL-microfiber substrates were sterilized by incubation in 70% ethanol for 20 min and rinsed with DPBS buffer and sterile water. After air-drying, the microfiber substrates were incubated at 4°C overnight with ECL at 10 μg/mL to facilitate cell attachment. Excess ECL was removed, and the PCL scaffolds were rinsed with DPBS. Scanning electron microscopy (SEM; JCM-6000 NeoScope Benchtop scanning electron microscope) was applied to characterize the PCL fibers. In order to acquire high-quality SEM images, the substrates were made conductive using gold sputter-coating. The coating thickness of the samples was approximately 50 nm. Approximately 30 fibers were chosen and characterized.

Live cell calcium signaling

To study the intracellular calcium signaling, the astrocytes were loaded with 5 μM Fluo-4 AM (Thermo Fisher Scientific, Waltham, MA) for 30 min at room temperature, rinsed three times with HBSS. Coverslip with Fluo-4 AM loaded astrocytes was mounted on the top of a custom-built chamber and immersed in an artificial cerebrospinal fluid (ACSF) (125 mM NaCl, 3 mM KCl, 10 mM glucose, 26 mM $NaHCO_3$, 1.1 mM NaH_2PO_4, 2 mM $CaCl_2$, 1 mM $MgSO_4$; pH adjusted to 7.4), and imaged using a 20x/NA 0.75 microscope objective and a sCMOS camera (Andor, UK). Fluorescence signals that represent the intracellular calcium concentration ($[Ca^{2+}]_i$) were monitored in real time at 5 s intervals for a period of 10 min. Average fluorescence intensities of each cell were determined using Image J (https://imagej.nih.gov/ij/) and its built-in segmentation tool. NucBlue™ Live Ready Probe was used to label the nuclei of astrocytes.

Results and Discussion

Two types of PCL fibers of different fiber diameters were fabricated by regulating the PCL solution flow rate from 1 to 5 μL/min and the sheath flow rate from 60 to 150 μL/min in the microfluidic channel. As shown in Figure 1, the type I fibers with average diameter and height of 30 and 20 μm, respectively, were found to be more uniform and controllable than the type 2 fibers (15 μm diameter and 10 μm height). Therefore the type I fibers were used in the subsequent experiments. However, our fabrication capability of the microfluidic fibers was nonetheless demonstrated to control and tune, if necessary, the size of the fibers by changing the flow rates. A bright field image of the type 1 fibers used in this paper is shown in Figure 1a. The fibers are seen to form a crisscross pattern with uniform fiber size and spatial regularity. To facilitate and enhance cell adhesion to the PCL fibers, the ECL cell attachment matrix was used to coat the surface of the fibers. Mouse astrocytes were guided to attach to the fibers only, as verified using the NucBlue fluorophores to visualize the nuclei (Figure 1b).

This cell seeding strategy allowed us to observe astrocytes attached to a single fiber. Mouse astrocytes loaded with the membrane permeable and calcium binding Fluo-4 AM were fluorescently identified. While it was evident that the PCL fibers exhibited autofluorescence, the Fluo-4 loaded cells provided detectable dynamic signals above the background signal that can be used to discriminate between the cells and fibers. We have compared the calcium wave between astrocytes attached the on a coverglass and astrocytes attached on PCL fibers. It was evident the calcium signals in astrocytes propagated omni-directionally on coverglass (Figure 2a) while they were observed to propagate in one particular direction along the PCL fibers (Figure 2b). This result indicated that the propagation direction of calcium signaling was successfully guided along the PCL fibrous network.

To examine the possible correlation of calcium signaling, three

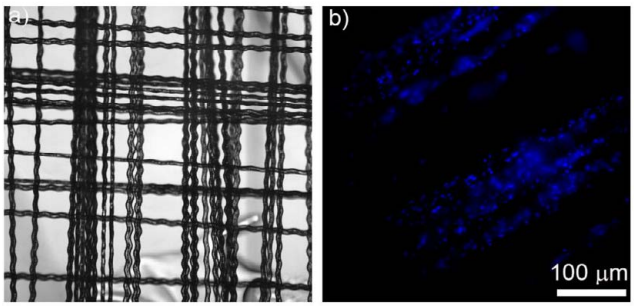

Figure 1: Bright field image of PCL fibers (a) and fluorescent image of nuclei of astrocytes seeded on the PCL fibers (b). Bar=100 μm. Average diameter of the fiber was 30 μm. Astrocytes were observed to attach on the fibers. A 20x air microscope objective was used to record the images.

astrocytes were specifically identified and monitored for transient calcium dynamics. The first astrocyte visualized on the fiber showed bright and fluctuating fluorescent intensity, indicating there was likely calcium spiking activity (shown in the black circle and denoted cell #1; Figure 3a). At a later time (~30 s), another cell showed calcium spiking (green circle; denoted cell #2; Figure 3b). This cell #2 was located at least a few cell lengths away from the cell #1 and showed no physical contact. We also captured the cell #3 (red circle; Figure 3c) that also demonstrated calcium spiking. Unlike the cell #2, this cell was either in contact with the cell #1 or within a distance from the cell #1 that allowed the possibility of communicating via secreted molecules. While it would be easier to provide an explanation of cells that are in contact, brain cells seeded in the range of diffusional distance are known to communicate via release of neurotransmitters [25] and thus cannot be simply ignored. This kind of challenge will be better elucidated in the future experiments. One improvement that can further clarify calcium dynamics in the cells in 3D PCL fiber would require elimination of the autofluorescence from the PCL fibers. The technical challenge can be mitigated using a newer class of red calcium-specific fluorophore that absorbs light at 573 nm and emits fluorescence signals at 588 nm (i.e., Calbryte™ 590, AAT Bioquest, Sunnyvale, CA). Successful calcium imaging using the Calbryte fluorophore has been reported [26]. Therefore, this spectrally well-separated fluorophore is expected to enhance the detection of calcium dynamics in astrocytes plated on the PCL fiber.

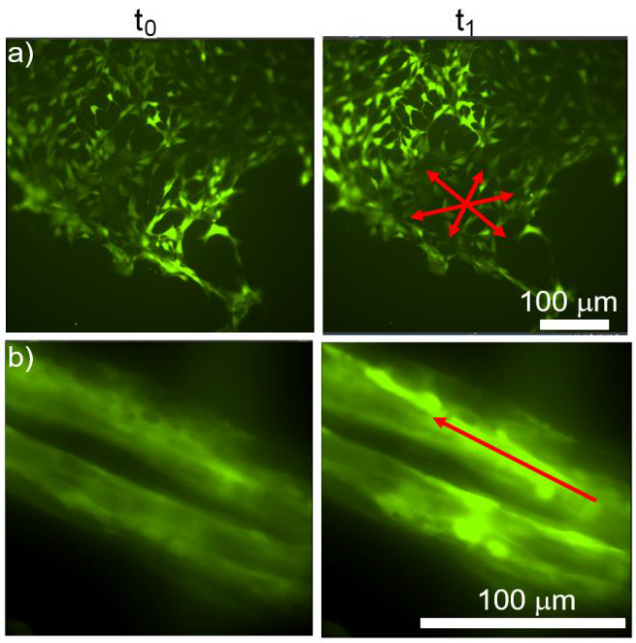

Figure 2: Comparison of propagation of calcium signals. Astrocytes were seeded on coverslip and loaded with calcium-specific Fluo-4 (a). The right panel shows the same cells recorded 372 s after the left panel image was captured. No defined direction of propagation of calcium signal was observed. In contrast, cells seeded on the PCL fibers show attachment along the axis of the fibers (b). Again the right panel show the same cells recorded 186 s later. A noticeable increase in the fluorescent intensity indicates transient calcium fluctuation.

Of the three astrocytes, the transient calcium spiking patterns of the cells were monitored and recorded in real-time. Because the fluorescent intensities can vary mainly due to the cell-dependent fluorophore loading efficiency, a better way to represent the spiking patterns is to normalize the fluorescence intensities by the maximum value of each of these cells. Such normalized profiles of the cell #1 and cell #3 are shown in Figure 3d. Guided by a sophisticated correlation analysis, referred to as the wavelet transform coherence (WTC; see below for an extended description), the two profiles would appear similar in the time domain and demonstrate a high correlation. Indeed, the calcium spiking pattern of the cell #1 (black circle cell) was shifted by 45 s and plotted together with that of the cell #3, demonstrating the likelihood of a correlation between these two cells. The same quantitative comparison was carried

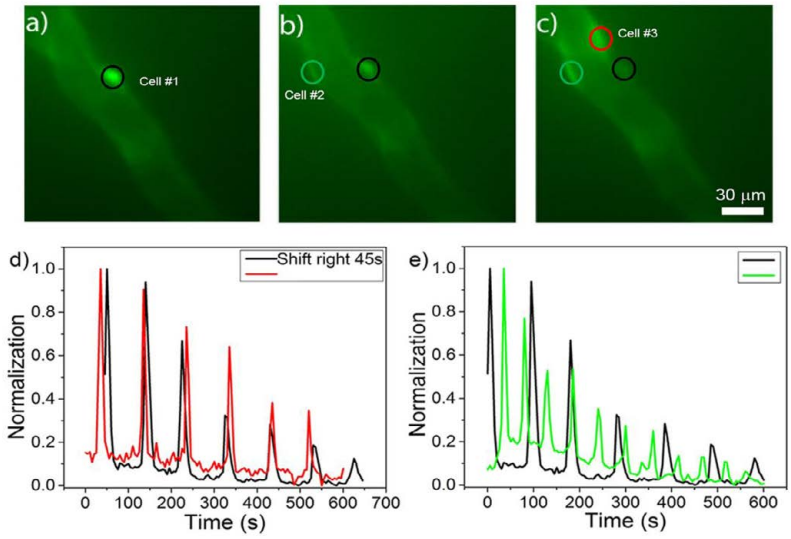

Figure 3: Cells were loaded with Fluo-4 and three adjacent cells seeded on a single PCL fiber was visualized. Only one cell exhibited a sufficient fluorescence intensity to be identified by the image processor (a; black circle). At a later time, two cells were identified (b; black and green circles). The cell identified in (a) showed a diminished fluorescence intensity. At a later time, two cells were visualized (c; green and red circles). The cell identified in (a) now showed the fluorescence intensity that is not above the background (e.g., autofluorescence). Based on monitoring changes of the fluorescence intensity in real time, the calcium spiking patterns were recorded. Since the Fluo-4 loading efficiency is variable, the normalized fluorescence intensities were plotted and shown. (d) shows the normalized intensities of the two cells (green and red circles). Guided by WTC analysis, the intensities from the black circle cell were offset by 45 s. The same analysis indicated the patterns of the black circle and green circle cells were negligibly correlated (no time shift).

out between the calcium spiking patterns of the cell #1 and #2 (Figure 3e). This pair of cells appeared to be weakly or negligibly correlated. A sophisticated analysis would be required to quantify the extent of correlation.

It is a rather a difficult task to estimate correlation of the transient calcium spiking behavior using traditional methods because the calcium spiking profiles are clearly non-stationary. A feasible mathematic analysis method, referred to as wavelet transform coherence (WTC), is used to establish the extent of correlation, i.e., plausible cell-to-cell communication through calcium spiking. WTC is a time-frequency domain analysis that characterizes the cross-correlation and relative phase between two signals [27]. This analysis method has been successfully implemented to study the dynamic cerebral autoregulation in newborns with hypoxic-ischemic encephalopathy [28] and children on extracorporeal member oxygenation [29]. Briefly, WTC quantifies the squared cross-wavelet coherence, R^2, and relative phase, $\Delta\varphi$, between two paired signals in the time-frequency domain [27]. R^2 ranging between 0 and 1 can be conceptualized as a localized correlation coefficient in the time-frequency domain and the rule of thumb for interpreting the size of a correlation coefficient is listed in Table 1. The relative phase between the two paired signals, $\Delta\varphi$, ranges between $-\pi$ and π. Specifically, $\Delta\varphi=0$ represents an in-phase correlation where the two signals oscillate without lagging, whereas $\Delta\varphi=\pi$ represents one of the two signals oscillates with a time lag that is a half of the time period. If $\Delta\varphi=\pi/2$ or $-\pi/2$, the two signals are likely asynchronous. Both R^2 and $\Delta\varphi$ are functions of the wavelet scale, s, which is inversely proportional to the Fourier frequency ($s \propto 1/f$). Compared with conventional analysis based on Pearson correlation coefficient [30], for example, WTC makes no stationary assumption and therefore is a more valid tool to analyze non-stationary and transient physiological signals [31].

In the two adjacent cells presumed to have established cell-to-cell communication (cells #1 and #3 shown in Figure 3), the WTC analysis produced a map of the central time ($T_{central}$) of 90 s and the phase angle of $\Delta\varphi=\pi$. The correlation analysis indicates the two cells are anti-correlated (e.g., the direction of the arrows is pointed to the left in the darker yellow region; Figure 4a). This suggested to us that if one of the calcium spiking pattern is shifted by 45 s in the time domain, one could illustrate a high degree of correlation (Figure 3d). The correlation coefficient between the two calcium spiking profiles was determined $R^2=0.75$ (high correlation; see Table 1). To further validate the usefulness of WTC analysis, we performed the same correlation analysis for the cell #1 and #2. Again a correlation map was generated (Figure 4b), which demonstrates a negligible correlation ($R^2=0.24$) and indicates asynchronous calcium spiking ($\Delta\varphi \sim \pi/2$).

Size of Correlation	Interpretation
0.90 to 1.00	Very high positive correlation
0.70 to 0.90	High positive correlation
0.50 to 0.70	Moderate positive correlation
0.30 to 0.50	Low positive correlation
0.00 to 0.30	Negligible correlation

Table 1: Classification of the correlation coefficient [30].

It is not unusual to observe synchronization of the calcium spiking between two adjacent cells that are in physical contact. To further study and expand the cell-to-cell communication behavior, we recorded the calcium dynamics of six cells along one PCL fiber and calculated the correlation coefficients and phase angles (Figure 5). The boundaries of the six cells were determined using a built-in module of image processor (Element, Nikon Corp). A total of 15 combinatory pairs were examined, and their correlation coefficients and the phase angles were calculated and tabulated. Only three pairs of cells showed high correlation of >0.75. A high correlation coefficient (0.83) between cell numbered 5 and 6 is not surprising because these two cells are likely in physical contact. However, one pair of cell #1 and #4 and another pair of cell #2 and #4 also showed high correlation coefficients (0.87 and 0.75, respectively), even though these cells appear not in physical contact (*detailed analyses of wavelet transform coherence similar to those shown in Figure 4 are available upon request*). Several explanations may be formulated. First, the PCL fiber may act as a conduit to facilitate cell communication. While this hypothesis can be validated or rejected by seeding cells on another biocompatible polymer, it is unlikely that the materials would mediate cell communication via calcium spiking. Second, different chemical environment may have contributed. Instead of coating the fibers with ECL matrix, one ECM protein could be used to coat the fibers. We are currently working with a collaborator who can fabricate collagen fibers of ~1.0 μm in diameter using Fountain Pen approach [32] to determine the role of the chemical environment. Third, it is more likely that the two pairs of cells showing a high correlation may have been undergoing calcium spiking independently and not been influenced by the other cell. In this scenario, the WTC analysis can serve as a good indicator of potential cell-cell communication through calcium signaling but it alone may not be a sufficient predictor. However, the analysis does provide a quantitative measure for non-stationary correlation of cells that are presumed to be in contact. While much more work would be required to fully understand the cell communication mechanisms in astrocytes, our

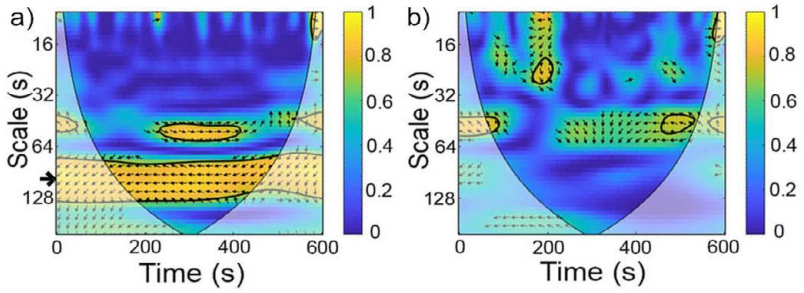

Figure 4: Analysis of coherence of the two corresponding traces (Figure 3d and 3e) using wavelet transform. In this graph the x-axis represents time t, the y-axis represents wavelet scale s (in inverse proportion to Fourier frequency, i.e., $s \propto 1/f$), and the color scale represents the squared cross-wavelet coherence R^2 that ranges from 0 to 1. The arrows designate the relative phase angle, $\Delta\varphi$. A rightward-pointing arrow indicates in-phase coherence ($\Delta=0$) and the leftward-pointing arrow indicates anti-phase coherence ($\Delta\varphi=\pi$). As shown in this analysis, the two signals are highly correlated at a central wavelet scale of $s_c \approx 90$ s, with a significant time lag of ~45 s (a). In contrast, the central wavelet scale remains indeterminate between the two traces shown in Figure 3e. The phase angle is approximately, $\Delta\varphi=\pi/2$, demonstrating these two traces are best described as not coherent at any wavelet scale (b).

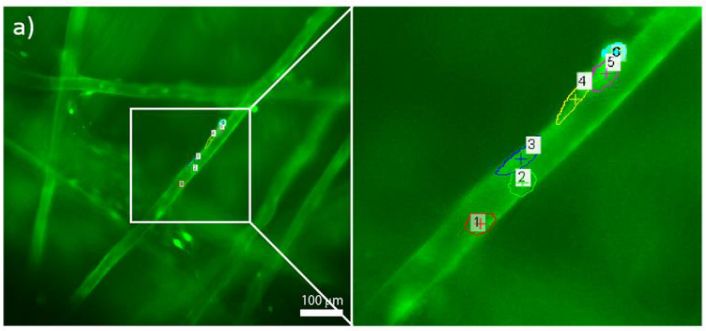

Central coherence

b)	1	2	3	4	5	6
1		0.56	0.40	0.87	0.29	0.57
2			0.53	0.75	0.60	0.59
3				0.47	0.51	0.62
4					0.44	0.56
5						0.83
6						

$\Delta\phi$ [Radian]

c)	1	2	3	4	5	6
1		0.74	0.54	0.39	1.13	0.98
2			1.21	1.31	0.83	0.50
3				0.13	1.27	0.48
4					0.07	0.67
5						0.54
6						

Δt [Sec]

d)	1	2	3	4	5	6
1		12.92	4.50	6.85	8.80	19.28
2			17.79	22.95	10.27	5.81
3				1.59	18.81	5.64
4					0.61	14.03
5						6.28
6						

Figure 5: Cells were loaded with the membrane permeable Fluo-4 AM, and six cells were selected to analyze the cell-to-cell communication. (a) Fluorescence image of six cells identified by the segmentation tool in the image processor (Element, Nikon). The mean coherence (b), relative phase angle (c), and time lag (d) were quantified at the central wavelet scale for each of the two paired cells. The central wavelet scale, s_c, was defined as the wavelet scale that shows the highest coherence over time between the two paired cells. Central coherence, relative phase, and time lag were calculated as the mean values over time at this scale.

experimental approaches combined with the WTC analysis method may pave an innovative way to study in depth the time-dependent cell-to-cell communication through calcium dynamic. As a specific example, experiments are currently underway to co-culture both astrocytes and neurons in a spatially designed configuration. Such an engineered biosystem should be proven useful to probe the cell-to-cell communication in a more physiologically relevant model using the WTC analysis. Moreover, it will also enable us to extend the scope of our studies by providing a microfluidic platform to examine the neurite growth in a controlled microenvironment, to test neurotoxicity and to facilitate drug discovery.

Conclusion

We have shown that PCL microfibers with different features can be engineered using microfluidic fabrication techniques. The cell-to-cell communication mediated by calcium signaling can be monitored and assessed by calculating the correlation coefficient between any pair of two cells in the region of interest. More detailed experiments are currently underway to elucidate whether spatially arranged cell seeding of neurons and astrocytes in the 3D microenvironment regulate neuronal communication via calcium signaling. This system could potentially lead to the development of engineered neural tissue constructs that may feature controlled neural network.

Acknowledgement

This work was supported by grants (N00014-16-1-2140; MC) and (N00014-16-1-2246; NH) from the Office of Naval Research.

References

1. Cheng H, Lederer W (2008) Calcium sparks. Physiol Rev 88: 1491-1545.
2. Barrige M, Bootman M, Roderick H (2003) Calcium signaling: dynamics, homeostasis, and remodeling. Nature 4: 517-529.
3. Small DH (2009) Dysregulation of calcium homeostasis in Alzheimer's disease. Neurochem Res 34: 1824-1829.
4. Kuga N, Sasaki T, Takahara Y, Matsuki N, Ikegaya Y (2011) Large-scale calcium waves traveling through astrocytic networks in vivo. J Neurosci 31: 2607-2614.
5. Kraft A, Jubal ER, von Laer R, Döring C, Rocha A, et al. (2017) Astrocytic calcium waves signal brain injury to neural stem and progenitor cells. Stem Cell Rep 8: 701-714.
6. Newman EA, Zahs KR (1997) Calcium waves in retinal glial cells. Science 275: 844-847.
7. Volterra A, Liaudet N, Savtchouk I (2014) Astrocyte Ca2+ signalling: an unexpected complexity. Nat Rev Neurosci 15: 327-335.
8. Nelson MT, Short A, Cole SL, Gross AC, Winter J, et al. (2014) Preferential, enhanced breast cancer cell migration on biomimetic electrospun nanofiber 'cell highways'. BMC Cancer 14: 825.
9. Schnell E, Klinkhammer K, Balzer S, Brook G, Klee D, et al. (2007) Guidance of glial cell migration and axonal growth on electrospun nanofibers of poly-ε-caprolactone and a collagen/poly-ε-caprolactone blend. Biomater 28: 3012-3025.
10. Wang X, Salick MR, Wang X, Cordie T, Han W, et al. (2013) Poly (ε-caprolactone) nanofibers with a self-induced nanohybrid shish-kebab structure mimicking collagen fibrils. Biomacromolecules 14: 3557-3569.
11. Leung M, Cooper A, Jana S, Tsao CT, Petrie TA, et al. (2013) Nanofiber-based in vitro system for high myogenic differentiation of human embryonic stem cells. Biomacromolecules 14: 4207-4216.
12. Omidvar N, Ganji F, Eslaminejad MB (2016) In vitro osteogenic induction of human marrow-derived mesenchymal stem cells by PCL fibrous scaffolds containing dexamethazone-loaded chitosan microspheres. J Biomed Mater Res Part A 104: 1657-1667.
13. Sharifi F, Patel BB, Dzuilko AK, Montazami R, Sakaguchi DS, et al. (2016) Polycaprolactone microfibrous scaffolds to navigate neural stem cells. Biomacromolecules 17: 3287-3297.
14. Ghasemi-Mobarakeh L, Prabhakaran MP, Morshed M, Nasr-Esfahani MH, Ramakrishna S (2008) Electrospun poly (ε-caprolactone)/gelatin nanofibrous scaffolds for nerve tissue engineering. Biomater 29: 4532-4539.
15. Cooper A, Bhattarai N, Zhang M (2011) Fabrication and cellular compatibility of aligned chitosan–PCL fibers for nerve tissue regeneration. Carbohydr Polym 85: 149-156.
16. Nisbet D, Yu L, Zahir T, Forsythe JS, Shoichet M (2008) Characterization of neural stem cells on electrospun poly (ε-caprolactone) submicron scaffolds: evaluating their potential in neural tissue engineering. J Biomater Sci Polym Ed 19: 623-634.
17. Daud MF, Pawar KC, Claeyssens F, Ryan AJ, Haycock JW (2012) An aligned 3D neuronal-glial co-culture model for peripheral nerve studies. Biomater 33: 5901-5913.

18. Sharifi F, Sooriyarachchi AC, Altural H, Montazami R, Rylander MN, Hashemi N (2016) Fiber based approaches as medicine delivery systems. ACS Biomater Sci Eng 2: 1411-1431.

19. Shi X, Ostrovidov S, Zhao Y, Liang X, Kasuya M, Kurihara K, et al. (2015) Microfluidic spinning of cell-responsive grooved microfibers. Adv Funct Mater 25: 2250-2259.

20. Daniele MA, Boyd DA, Adams AA, Ligler FS (2015) Microfluidic strategies for design and assembly of microfibers and nanofibers with tissue engineering and regenerative medicine applications. Adv Healthcare Mater 4: 11-28.

21. Sharifi F, Bai Z, Montazami R, Hashemi N (2016) Mechanical and physical properties of poly (vinyl alcohol) microfibers fabricated by a microfluidic approach. RSC Advances 6: 55343-55353.

22. Sharifi F, Kurteshi D, Hashemi N (2016) Designing highly structured polycaprolactone fibers using microfluidics. J Mech Behav Biomed Mater 61: 530-540.

23. Sun S, Kanagaraj J, Cho L, Kang D, Xiao S, Cho M (2015) Characterization of subcellular responses induced by exposure of microbubbles to astrocytes. Journal of Neurotrauma 32: 1441-1448.

24. Kanagaraj J, Chen B, Xiao S, Cho M (2018) Reparative effects of poloxamer P188 in astrocytes exposed to controlled microcavitation. Ann Biomed Eng 46: 354-364.

25. Yarom M, Zurgil N, Zisapel N (1985) Calcium permeability changes and neurotransmitter release in cultured brain neurons. II. Temporal analysis of neurotransmitter release. J Biol Chem 260: 16294-16302.

26. Tischbirek C, Birkner A, Jia H, Sakmann B, Konnerth A (2015) Deep two-photon brain imaging with a red-shifted fluorometric Ca2+ indicator. Proc Natl Acad Sci 112: 11377-11382.

27. Grinsted A, Moore JC, Jevrejeva S (2004) Application of the cross wavelet transform and wavelet coherence to geophysical time series. Nonlinear Processes in Geophysics 11: 561-566.

28. Tian F, Tarumi T, Liu H, Zhang R, Chalak L (2016) Wavelet coherence analysis of dynamic cerebral autoregulation in neonatal hypoxic–ischemic encephalopathy. NeuroImage: Clinical 11: 124-132.

29. Tian FH, Morriss MC, Chalak L, Venkataraman R, Ahn C, et al. (2017) Impairment of cerebral autoregulation in pediatric extracorporeal membrane oxygenation associated with neuroimaging abnormalities. Neurophotonics 4: 041410.

30. Mukaka MM (2012) A guide to appropriate use of correlation coefficient in medical research. Malawi Medical Journal 24: 69-71.

31. Garg A, Xu D, Blaber AP (2013) Statistical validation of wavelet transform coherence method to assess the transfer of calf muscle activation to blood pressure during quiet standing. Biomedical Engineering Online 12: 1-14.

32. Je JH, Kim JM, Jaworski J (2017) Progression in the fountain pen approach: from 2D writing to 3D free-form micro/nanofabrication. Small 13: 1600137.